Hindawi Publishing Corporation
Journal of Nanomaterials
Volume 2013, Article ID 640940, 6 pages
http://dx.doi.org/10.1155/2013/640940

Research Article

Sol-Gel Synthesized Magnetic $MnFe_2O_4$ Spinel Ferrite Nanoparticles as Novel Catalyst for Oxidative Degradation of Methyl Orange

Linfeng Zhang[1] and Yuanxin Wu[1,2]

[1] *School of Chemical Engineering and Technology, Tianjin University, Tianjin 300072, China*
[2] *Key Laboratory for Green Chemical Process of Ministry of Education, Wuhan Institute of Technology, Wuhan 430073, China*

Correspondence should be addressed to Yuanxin Wu; wyx@mail.wit.edu.cn

Received 13 November 2013; Accepted 28 November 2013

Academic Editor: Amir Kajbafvala

The $MnFe_2O_4$ spinel ferrite nanoparticles with sensitive magnetic response properties and high specific surface area were prepared from metal nitrates by the sol-gel process as catalysts for oxidative degradation of methyl orange (MO). The nanoparticles were characterized by X-ray powder diffraction (XRD), scanning electron microscopy (SEM), BET surface area analysis, H_2-Temperature programmed reduction (H_2-TPR), X-ray photoelectron spectra (XPS), and vibration sample magnetometer (VSM). The catalytic activity experimental results showed that the $MnFe_2O_4$ spinel ferrite nanoparticles possess very high MO degradation activity. It is expected that this kind of $MnFe_2O_4$ spinel ferrite nanoparticles has a potential application in water treatment fields due to its sensitive magnetic response properties and high catalytic activity.

1. Introduction

Recently, synthetic organic dyes and pigments are widely used in the textiles, paper, plastics, leather, food, and cosmetic industry to color the products [1]. Usually, the synthetic organic dyes are nonbiodegradable and hence cause a serious threat to our ecology environment and human health. Among various classes of dyes, the azo dyes represent a major group of dyes and have been widely applied in textile industries because of their ease of synthesis, versatility, and cost effectiveness [2]. However, due to the strong toxicity and the high solubility of these dyes, varieties of methods are proposed for the removal of them such as adsorption, filtration, sedimentation, and catalytic action [3]. Among these methods, the catalytic degradation method, assisted with optical radiation or strong oxidizer, has been demonstrated as one of the important, innovative, and green technologies. In the catalytic degradation process, using semiconductors [4–7] and multicomponent oxides [8, 9] as the catalysts to degrade azo dye has attracted extensive attention. However, the separation of these catalysts from treated water, especially from a large volume of water, is expensive and time consuming, which limited their application in industrial fields. It is realized that introducing the magnetic catalysts is a good choice to deal with the catalysts separation and reuse problems.

Among various of magnetic oxides, the ferrite MFe_2O_4 (M = Mn, Co, Zn, Mg, Ni, etc.) is a well-known cubic spinel material where oxygen forms a face-centered cubic (fcc) close packing, and M^{2+} and Fe^{3+} occupy either tetrahedral or octahedral interstitial sites [10, 11]. Due to its stable crystal structure and good magnetic properties, it has been widely used in electronic devices, information storage, magnetic resonance imaging (MRI), and drug-delivery technology [12–14]. Manganese spinel ferrite ($MnFe_2O_4$) with good magnetism and functional surface was widely used as an adsorbent for removing heavy metals in water solution [15]. However, few studies were focused on azo dyes oxidative degradation process by directly employing $MnFe_2O_4$ nanoparticles as catalyst. Regarding the synthesis method, there are many methods, such as sol-gel, coprecipitation, microemulsion, solid state reaction and other techniques have been reported. Among these methods, sol-gel method is a low-cost and effective way to prepare nanoscale $MnFe_2O_4$ at a low temperature [16]. In this paper, the $MnFe_2O_4$ nanoparticles with sensitive

magnetic response properties and high specific surface area were prepared from metal nitrates by sol-gel process and afterwards used as a catalyst to oxidative degrade of methyl orange (MO) in the aqueous solution. The characteristics of the nanoparticles were studied by XRD, BET, SEM, H_2-TPR, XPS, and VSM analyses. The reason for the high degradation activity of the catalyst was also analyzed.

2. Materials and Methods

2.1. Material Preparation. $MnFe_2O_4$ spinel ferrites nanoparticles were prepared by the sol-gel method. Stoichiometric amounts of $Mn(NO_3)_2$ (50% solution) and $Fe(NO_3)_3{\cdot}9H_2O$ powder were mixed with a certain amount of deionized water. The citric acid as the complexing agent was then added to the metal nitrate solution with a molar ration of 1 : 1. Then the resulting solution was evaporated to dryness, and thereafter the precursor was decomposed at 200°C until dry gel was formed. Finally, the residual precursor was calcined in air at 400, 500, 600, 700, and 800°C for 2 h and the obtained $MnFe_2O_4$ nanoparticles were signed as MNF-400, MNF-500, MNF-600, MNF-700, and MNF-800.

2.2. Characterizations. The phase identification and crystalline structure analysis were determined by X-ray diffraction (XRD) using a Panalytical X-pert diffractometer (PANalytical, Netherlands) with a Cu Kα radiation (λ = 0.154056 nm) operated at 40 kV and 30 mA. The surface area (S_{BET}) of the nanoparticles was calculated from the nitrogen adsorption isotherms obtained at 77 K by using a NOVA2000e apparatus. Scanning electron microscopy (SEM) (JEOL, Model JSM-5510LV) was used to investigate the morphology of the derived nanoparticles. H_2-Temperature programmed reduction (H_2-TPR) experiments were performed in a quartz reactor using a thermal conductivity detector (TCD) as a detector on Micromeritics AutoChem 2920 instrument. The chemical shift and valence of element on surface were examined by X-ray photoelectron spectra (XPS) in a Perkin-Elmer PHI 1600 ESCA system with Mg Kα X-ray radiation (1253.6 eV, 150 W). The binding energies were calibrated using *C1s* peak at 284.6 eV. The magnetic properties of the nanoparticles were measured at room temperature through a HH-10 vibration sample magnetometer (VSM). The light absorption spectrum of the MO solution was detected by U-2102 UV-Vis spectrophotometer (UNICO, USA) at 507 nm [17].

2.3. Catalytic Activity Test. 0.1 g $MnFe_2O_4$ nanoparticles were added to 200 ml methyl orange (MO) solution (30 mg·L^{-1}). Then the aqueous suspension was stirred for 30 min to obtain better dispersion and adsorption performance prior to the degradation. The pH value of the MO solution was adjusted to 3 by adding hydrochloric acid and then 1 ml H_2O_2 was dropped in as the oxidant. At degradation time intervals of 0.5 h, a small quantity of solution was taken from the test solution and analyzed by measuring the absorbance at 507 nm by a spectrophotometer. Consequently, the degradation rate of MO could be calculated as follow [18]: $D(\%) = ((C_i - C_t)/C_i) \times 100$, where D was the degradation rate of MO, the C_i was the initial concentration of MO, and C_t was concentration of MO at time t.

3. Results and Discussion

3.1. XRD and Structure Analysis. Figure 1 showed XRD patterns (a) and SEM images (b, c, d) of $MnFe_2O_4$ nanoparticles obtained from different precursor's calcination temperatures (b-MNF-400; c-MNF-500; d-MNF-600). Figure 1(a) showed the XRD patterns of the $MnFe_2O_4$ nanoparticles. When the calcination temperature was 400°C, the obtained $MnFe_2O_4$ nanoparticle has the single crystalline phase, while at 500°C, the intensity of each characteristic peak increased significantly, and the crystalline phase of ferrite tended to be more complete. Nevertheless, when the calcination temperature was above 600°C, some miscellaneous phase peaks appeared in the obtained $MnFe_2O_4$ spinel ferrite nanoparticles. Meanwhile,the miscellaneous phase peak intensity increased constantly with the decrease of the characteristic peak intensity of original ferrite as the calcination temperature rose. Compared to the standard card (JCPDS 33-0664), it could be inferred that the obtained $MnFe_2O_4$ spinel ferrite nanoparticles were partly dissolved into Fe_2O_3 as the precursor was calcinated in oxygen-rich atmospheres at higher temperature.

The surface area measurements results showed that the specific surface areas of $MnFe_2O_4$ nanoparticles declined with the increase of the calcination temperature. When the calcination temperature rose from 400 to 800°C, the specific surface area of the obtained $MnFe_2O_4$ nanoparticles decreased from 52.6 to 5.8 $m^2{\cdot}g^{-1}$. Moreover, Figures 1(b), 1(c), and 1(d) showed the SEM images of the $MnFe_2O_4$ nanoparticles obtained from different precursor's calcination temperatures. From Figure 1(c), we could see that the uniform and large apertures with obvious networks structure were present in the MNF-500 nanoparticles. Figure 1(b) showed that the pore structure of the MNF-400 nanoparticles has not yet formed completely, in which the aperture was not as large as the MNF-500 nanoparticles. Nevertheless, it could be seen from Figure 1(d) that the surface of the MNF-600 nanoparticles sintered and the surface pore structure collapsed with the increasing calcination temperature, and the specific surface area decreased sharply. The MNF-500 showed well crystal structure and uniform pore structure with larger specific surface areas compared to other MNF nanoparticles.

3.2. H_2-TPR Analysis. In this paper, the redox behavior of the obtained MNF nanoparticles was investigated by H_2-Temperature Programmed Reduction (H_2-TPR). Figure 2 showed the H_2-TPR profiles of the $MnFe_2O_4$ nanoparticles obtained from different precursor's calcination temperatures. It could be seen that there were three reduction peaks in the H_2-TPR spectra of the MNF-500 nanoparticles. The corresponding redox potential of each metal ion $\varphi_{MnO_2/Mn^{2+}}$, $\varphi_{Mn^{3+}/Mn^{2+}}$, $\varphi_{Mn^{2+}/Mn}$, $\varphi_{Fe^{3+}/Fe^{2+}}$, and $\varphi_{Fe^{2+}/Fe}$ was +1.224 eV, +1.51 eV, −1.186 eV, +0.771 eV, and −0.4402 eV, respectively. It turned out that it is difficult for MnO to be reduced under the present experimental conditions and there was no reducing process of MnO. So the reducing process could

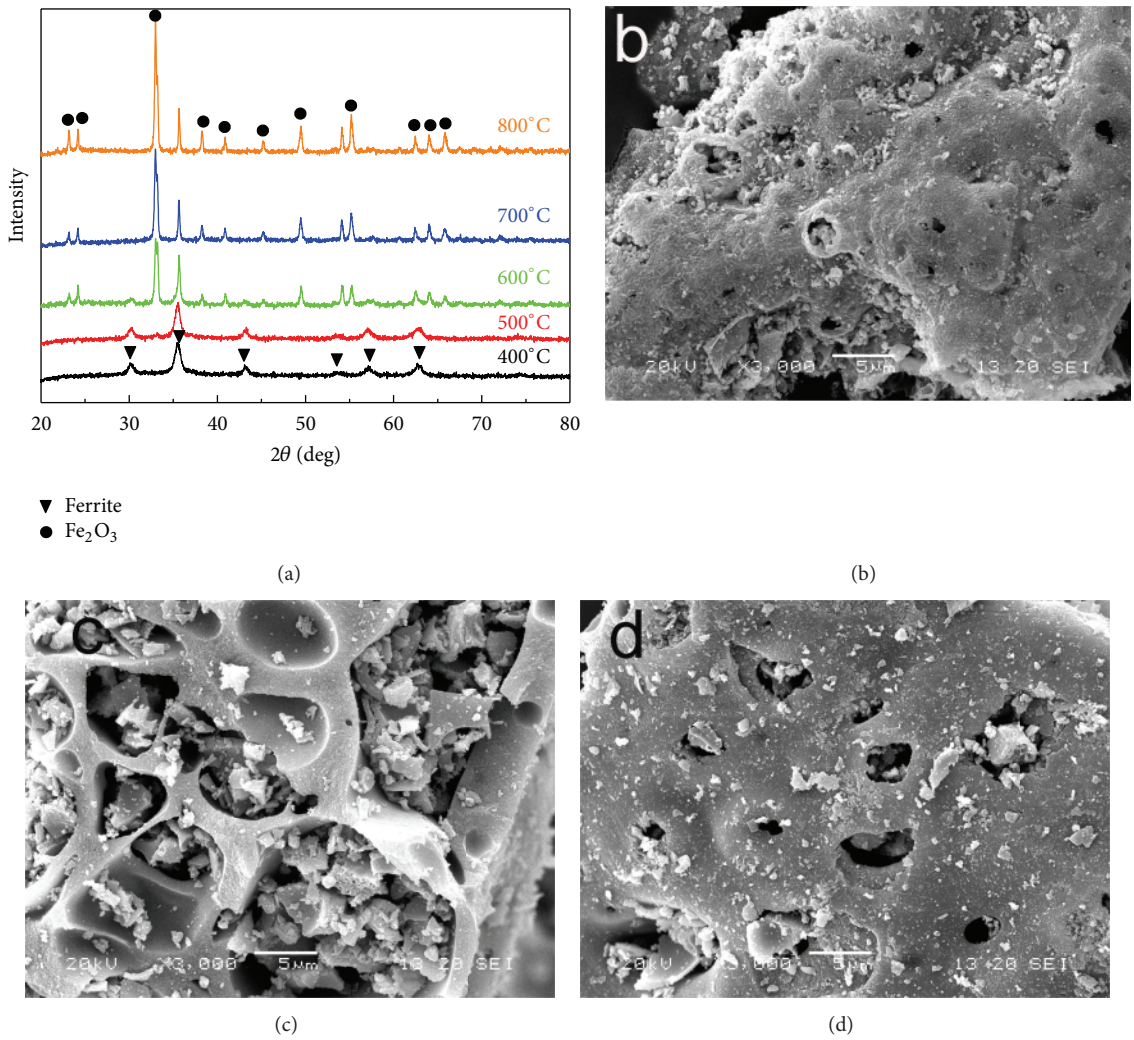

FIGURE 1: XRD patterns (a) and SEM images (b, c, and d) of $MnFe_2O_4$ nanoparticles obtained from different precursor's calcination temperatures (b-MNF-400; c-MNF-500; d-MNF-600).

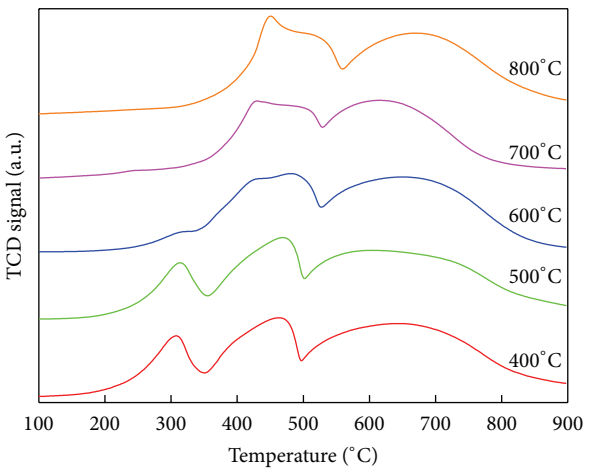

FIGURE 2: H_2-TPR profiles of $MnFe_2O_4$ nanoparticles obtained from different precursor's calcination temperatures (at 400, 500, 600, 700, and 800°C, resp.).

be inferred as $MnFe_2O_4 \rightarrow MnFe_2O_{4-\delta} \rightarrow$ MnO-FeO solid solution$\rightarrow \alpha$-Fe. When the calcination temperature was over 600°C, the reduction peak around 310°C tended to be weak or even disappeared, whereas a new reduction peak around 430°C which was formed as an acromion with the reduction peak around 490°C turned up and gradually strengthened. It is supposed that, when the calcination temperature was over 600°C, spinel structure of the $MnFe_2O_4$ was destroyed and the new phase Fe_2O_3 was formed. Additionally, as the calcination temperature rose up, this transition tended to be more obvious. Therefore as the calcination temperature rose, besides $MnFe_2O_4$ ferrite, Fe_2O_3 as a newly formed structure appeared in the sample, which could change the reducing property of the obtained nanoparticles. The impact of calcination temperature on the redox property of the MNF nanoparticles was consistent with that on the XRD characterization results. The lower the initial reduction peak temperature was, the much easier the MNF nanoparticles changed into oxygen deficient ferrite $MnFe_2O_{4-\delta}$ would, therefore the

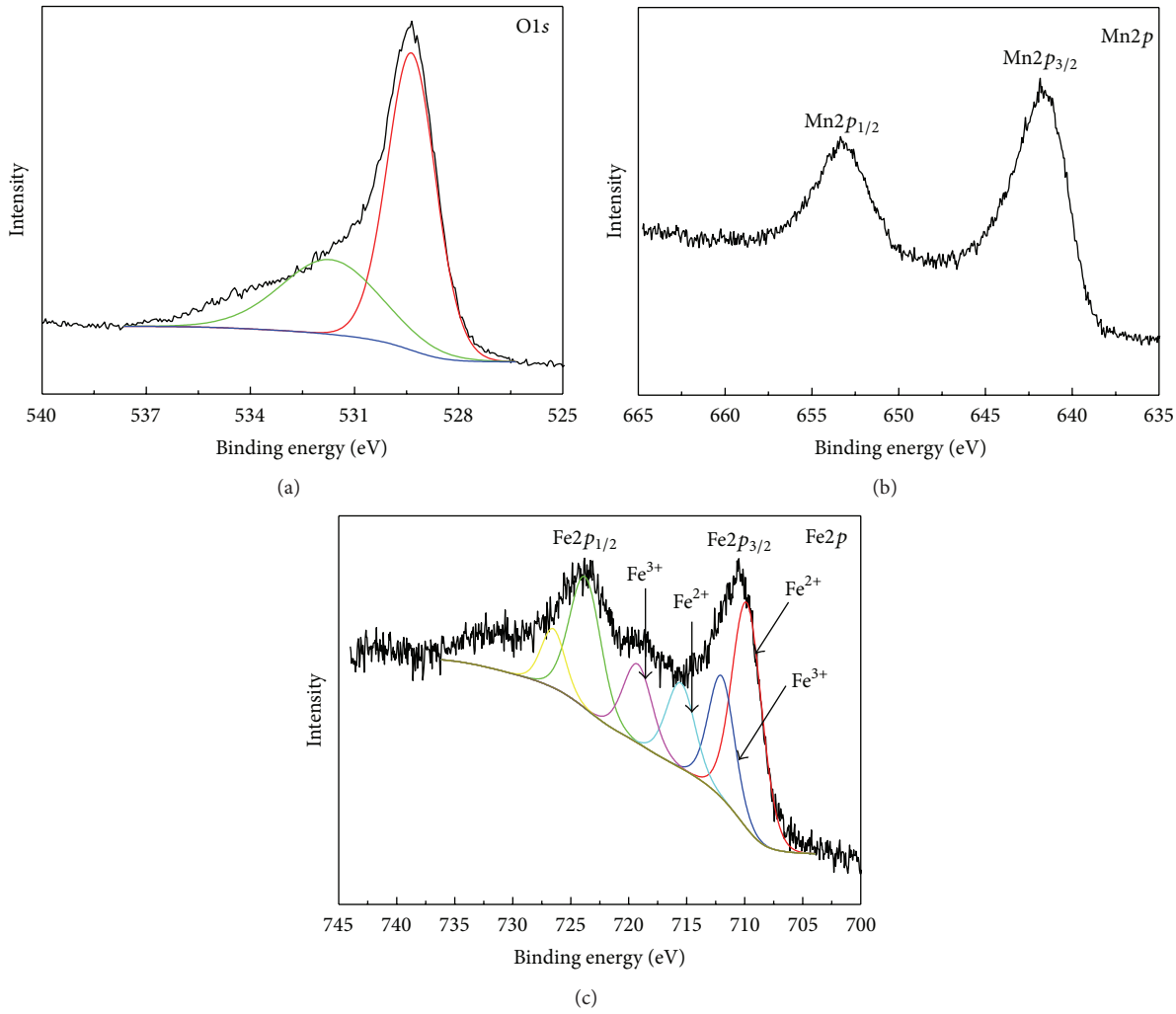

FIGURE 3: Core level XPS spectra of the MNF-500 nanoparticles: (a) O1*s*, (b) Mn2*p*, and (c) Fe2*p*.

redox property of it was better [19]. Therefore the $MnFe_2O_4$ nanoparticles which were obtained form a lower precursor calcination temperature may show better low-temperature oxidation performance than the ones obtained from a higher calcination temperature.

3.3. XPS Analysis. Figure 3 represented the XPS core level spectra of O1*s*, Mn2*p*, and Fe2*p* of the MNF-500 nanoparticles. Two photoemission peaks which correspond to two distinct oxygen species were illustrated in Figure 3(a). The line with low binding energy (about 529.5 eV) was attributed to the crystal lattice oxygen (O^{2-}); the high binding energy (about 531.3 eV) was attributed to active adsorbed molecular oxygen (O_2). Due to the defects of the lattice oxygen, large amounts of oxygen vacancies were produced so the adsorbed oxygen increased [20].

The Mn$2p_{3/2}$ and Mn$2p_{1/2}$ core-level emission peaks were observed at 641.5 eV and 653.0 eV in Figure 3(b). Thus, the Mn$2p_{3/2}$ peak was observed between those of MnO (641 eV) and Mn_2O_3 (641.6 eV) and the energy separation between the Mn$2p_{3/2}$ and Mn$2p_{1/2}$ states was 11.5 eV [21]. It could be inferred from the peak positions and the intensity ratio of Mn$2p_{3/2}$ and Mn$2p_{1/2}$ that the manganese existed as Mn^{2+} and Mn^{3+} states in the MNF-500 nanoparticles.

The Fe^{2+} $2p_{3/2}$ peak at 709.5 eV is always associated with a satellite peak at 6.0 eV above the principal peak whereas Fe^{3+} $2p_{3/2}$ peak at 711.2 eV is associated with a satellite peak at 8.0 eV [22]. In the MNF-500 nanoparticles, the binding energy values of Fe$2p_{3/2}$ were observed at 711.2 and 709.7 eV from Figure 3(c), and distinct satellite peaks were observed at about 8.0 eV and 6 eV above the main peak. Therefore the presence of Fe^{3+} and Fe^{2+} states could be confirmed in the MNF-500 nanoparticles.

3.4. Magnetic Measurements. Figure 4(a) showed the hysteresis loops of $MnFe_2O_4$ nanoparticles obtained from different calcination temperatures. The saturation magnetization of MNF-500 nanoparticles was 43.1 $A \cdot m^2 \cdot kg^{-1}$, which was the highest one compared to that of the other MNF nanoparticle. From the XRD patterns, the obtained $MnFe_2O_4$ nanoparticles were almost completely converted to nonmagnetic Fe_2O_3 when the calcination temperature was over 600°C. This phase transformation led to the sharp decline of the saturation

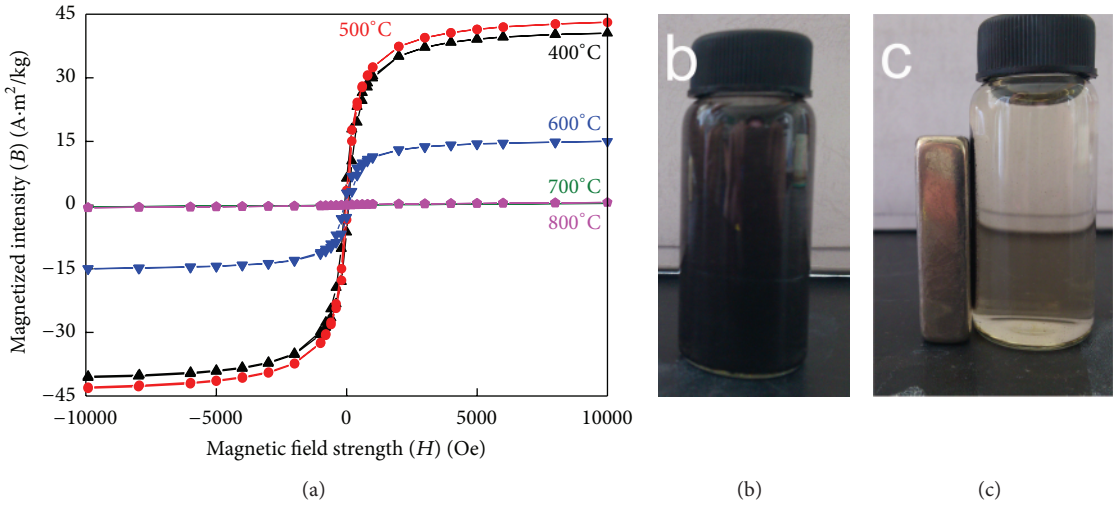

FIGURE 4: The hysteresis loops (a) of MNF nanoparticles and the magnetic response properties (b, c) of the MNF-500 in MO solution under an external magnetic field.

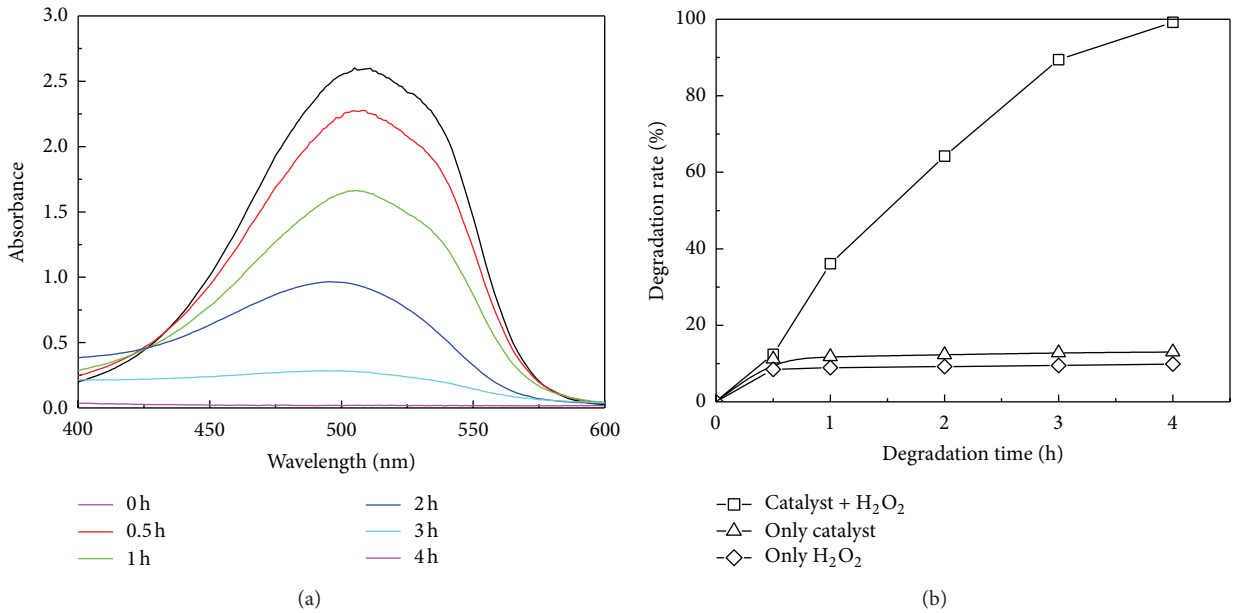

FIGURE 5: UV-Vis spectral evolution (a) of MO solution with reaction time (C_0 = 30 mg·L^{-1}, pH = 3.0, and H_2O_2 = 1 mL) and the degradation efficiency (b) of MO catalyzed by MNF-500 nanoparticles.

magnetization of the MNF nanoparticles. The remanent magnetization and coercivity of the obtained $MnFe_2O_4$ nanoparticles was low, indicating that all of them accorded with the properties of the soft magnetic material. The high saturation magnetization and soft magnetic property of the MNF-500 nanoparticles made them easy to separate from the aqueous suspension by an external magnetic field, as shown in Figures 4(b) and 4(c).

3.5. Oxidative Degradation Activity Test. Figure 5 showed the UV-Vis spectra evolution and degradation efficiency of MO catalyzed by the MNF-500 nanoparticles. With the catalytic reaction processing, the intensity of the characteristic peak of MO decreased gradually. After 4 h, the peak almost disappeared, while there was no appearance of any new adsorption peaks and shiftiness of the significant peak, meaning that 98% MO has been degraded. The high catalytic activity might attribute to the high specific surface area and the active absorbed oxygen species. In addition, the ion transference between different valences states of Mn and Fe in the nanoparticles was helpful for the degradation process. Therefore, it could be concluded that the MNF-500 nanoparticles exhibited excellent oxidative degradation activity for MO.

4. Conclusions

The $MnFe_2O_4$ spinel ferrite (MNF) nanoparticles were prepared from metal nitrates by the sol-gel process followed by a calcination at different temperatures. Comparing to the other MNF nanoparticles, the MNF-500 nanoparticles had a single crystalline phase; its specific surface area was 50.2 $m^2 \cdot g^{-1}$, and had better low-temperature oxidation activity. Due to the large number of active oxygen species on the surfaces and the ion transference of Mn and Fe, the MNF-500 nanoparticles showed a high MO degradation efficiency up to 98%. Additionally, the saturation magnetization of the MNF-500 nanoparticles was 43.1 $A \cdot m^2 \cdot kg^{-1}$ which made them easy to separate from the MO solution by an external magnetic filed. Thus this kind of $MnFe_2O_4$ nanoparticles will have a potential for oxidative degradation of dye in the water treatment fields.

Acknowledgments

This work was supported by the Key Program of National Natural Science Foundation of China (20936003) and the Foundation for Innovation Research Groups of the Natural Science Foundation of Hubei Province (2008CDA009).

References

[1] M. R. Hoffmann, S. T. Martin, W. Choi, and D. W. Bahnemann, "Environmental applications of semiconductor photocatalysis," *Chemical Reviews*, vol. 95, no. 1, pp. 69–96, 1995.

[2] R. Kumar, G. Kumar, and A. Umar, "ZnO nano-mushrooms for photocatalytic degradation of methyl orange," *Materials Letters*, vol. 97, pp. 100–103, 2013.

[3] A. Kajbafvala, H. Ghorbani, A. Paravar, J. P. Samberg, E. Kajbafvala, and S. K. Sadrnezhaad, "Effects of morphology on photocatalytic performance of Zinc oxide nanostructures synthesized by rapid microwave irradiation methods," *Superlattices and Microstructures*, vol. 51, no. 4, pp. 512–522, 2012.

[4] A. Kajbafvala, M. R. Shayegh, M. Mazloumi et al., "Nanostructure sword-like ZnO wires: rapid synthesis and characterization through a microwave-assisted route," *Journal of Alloys and Compounds*, vol. 469, no. 1-2, pp. 293–297, 2009.

[5] A. Kajbafvala, S. Zanganeh, E. Kajbafvala, H. R. Zargar, M. R. Bayati, and S. K. Sadrnezhaad, "Microwave-assisted synthesis of narcis-like zinc oxide nanostructures," *Journal of Alloys and Compounds*, vol. 497, no. 1-2, pp. 325–329, 2010.

[6] M. Mazloumi, S. Zanganeh, A. Kajbafvala et al., "Ultrasonic induced photoluminescence decay in sonochemically obtained cauliflower-like ZnO nanostructures with surface 1D nanoarrays," *Ultrasonics Sonochemistry*, vol. 16, no. 1, pp. 11–14, 2009.

[7] A. Kajbafvala, J. P. Samberg, H. Ghorbani, E. Kajbafvala, and S. K. Sadrnezhaad, "Effects of initial precursor and microwave irradiation on step-by-step synthesis of zinc oxide nanoarchitectures," *Materials Letters*, vol. 67, no. 1, pp. 342–345, 2012.

[8] L. Ge and J. Liu, "Efficient visible light-induced photocatalytic degradation of methyl orange by QDs sensitized CdS-Bi_2WO_6," *Applied Catalysis B*, vol. 105, no. 3-4, pp. 289–297, 2011.

[9] H. Fu, L. Zhang, W. Yao, and Y. Zhu, "Photocatalytic properties of nanosized Bi_2WO_6 catalysts synthesized via a hydrothermal process," *Applied Catalysis B*, vol. 66, no. 1-2, pp. 100–110, 2006.

[10] H. R. Zargar, M. R. Bayati, H. R. Rezaie et al., "Influence of nano boehmite on solid state reaction of alumina and magnesia," *Journal of Alloys and Compounds*, vol. 507, no. 2, pp. 443–447, 2010.

[11] P. Xiong, L. Wang, X. Sun et al., "Ternary titania-cobalt ferrite-polyaniline nanocomposite: a magnetically recyclable hybrid for adsorption and photodegradation of dyes under visible light," *Industrial & Engineering Chemistry Research*, vol. 52, pp. 10105–10113, 2013.

[12] S. Seifikar, B. Calandro, E. Deeb et al., "Structural and magnetic properties of biaxially textured $NiFe_2O_4$ thin films grown on c-plane sapphire," *Journal of Applied Physics*, vol. 112, pp. 123910–123914, 2012.

[13] S. Seifikar, A. Tabei, E. Sachet et al., "Growth of (111) oriented $NiFe_2O_4$ polycrystalline thin films on Pt (111) via sol-gel processing," *Journal of Applied Physics*, vol. 112, pp. 063908–063913, 2012.

[14] S. Shafiu, R. Topkaya, A. Baykal, and M. S. Toprak, "Facile synthesis of PVA-$MnFe_2O_4$ nanocomposite: its magnetic investigation," *Materials Research Bulletin*, vol. 48, pp. 4066–4071, 2013.

[15] Y. Ren, N. Li, J. Feng et al., "Adsorption of Pb(II) and Cu(II) from aqueous solution on magnetic porous ferrospinel $MnFe_2O_4$," *Journal of Colloid and Interface Science*, vol. 367, no. 1, pp. 415–421, 2012.

[16] J. Li, H. Yuan, G. Li, Y. Liu, and J. Leng, "Cation distribution dependence of magnetic properties of solgel prepared $MnFe_2O_4$ spinel ferrite nanoparticles," *Journal of Magnetism and Magnetic Materials*, vol. 322, no. 21, pp. 3396–3400, 2010.

[17] T. Fukuda, Y. Maeda, and H. Kitano, "Stereoselective inclusion of DOPA derivatives by a self-assembled monolayer of thiolated cyclodextrin on a gold electrode," *Langmuir*, vol. 15, no. 5, pp. 1887–1890, 1999.

[18] J. Zheng, H. Yu, X. Li, and S. Zhang, "Enhanced photocatalytic activity of TiO_2 nano-structured thin film with a silver hierarchical configuration," *Applied Surface Science*, vol. 254, no. 6, pp. 1630–1635, 2008.

[19] M.-S. Fu, L.-S. Chen, and S.-Y. Chen, "Preparation, structure of doped ferrite and its performance of decomposition of carbon dioxide to carbon," *Chemical Journal of Chinese Universities*, vol. 26, no. 12, pp. 2279–2283, 2005.

[20] M. A. Peluso, L. A. Gambaro, E. Pronsato, D. Gazzoli, H. J. Thomas, and J. E. Sambeth, "Synthesis and catalytic activity of manganese dioxide (type OMS-2) for the abatement of oxygenated VOCs," *Catalysis Today*, vol. 133–135, no. 1–4, pp. 487–492, 2008.

[21] C. V. Ramana, M. Massot, and C. M. Julien, "XPS and Raman spectroscopic characterization of $LiMn_2O_4$ spinels," *Surface and Interface Analysis*, vol. 37, no. 4, pp. 412–416, 2005.

[22] M. Vijayaraj and C. S. Gopinath, "On the "Active spacer and stabilizer" role of Zn in $Cu_{1-x}Zn_xFe_2O_4$ in the selective mono-N-methylation of aniline: XPS and catalysis study," *Journal of Catalysis*, vol. 241, no. 1, pp. 83–95, 2006.